A Parallel Reaction-Transport Model Applied to Cement Hydration and Microstructure Development

Jeffrey W. Bullard,[1] Edith Enjolras[2], William L. George,[2] Steven G. Satterfield[2], and Judith E. Terrill[2]

[1] Materials and Construction Research Division and [2] Mathematical and Computational Sciences Division, National Institute of Standards and Technology, Gaithersburg, Maryland USA

E-mail: jeffrey.bullard@nist.gov

Abstract. A recently described stochastic reaction-transport model on three-dimensional lattices is parallelized and is used to simulate the time-dependent structural and chemical evolution in multicomponent reactive systems. The model, called HydratiCA, uses probabilistic rules to simulate the kinetics of diffusion, homogeneous reactions, and heterogeneous phenomena such as solid nucleation, growth, and dissolution in complex three-dimensional systems. The algorithms require information only from each lattice site and its immediate neighbors, and this localization enables the parallelized model to exhibit near-linear scaling up to several hundred processors. Although applicable to a wide range of material systems, including sedimentary rock beds, reacting colloids, and biochemical systems, validation is performed here on two minerals that are commonly found in portland cement paste, calcium hydroxide and ettringite, by comparing their simulated dissolution or precipitation rates far from equilibrium to standard rate equations, and also by comparing simulated equilibrium states to thermodynamic calculations, as a function of temperature and pH. Finally, we demonstrate how HydratiCA can be used to investigate microstructure characteristics, such as spatial correlations between different condensed phases, in more complex microstructures.

PACS numbers: 82.20.Wt, 82.20.Na, 82.20.Nk

Submitted to: *Modelling Simulation Mater. Sci. Eng.*

1. Introduction

Understanding and predicting chemical and microstructural evolution in cement paste is a long-standing objective in concrete technology. The coupled dissolution and precipitation reactions that occur when cement powder is mixed with water determine a number of properties that are practically important, such as the setting time and the rate of heat release of concrete. Increased understanding of the mechanisms and rates of hydration reactions that occur in the first hours after mixing, as well as the development of microstructure, could lead to advances in the design and deployment of chemical admixtures for controlling these "early-age" properties. Better ability to predict the early-age properties of concrete could allow more informed decisions in the field about how to transport and place the material in service.

Accurate prediction of early-age properties of concrete with arbitrary mixture proportions and chemical composition requires a model that can simulate the rates of the coupled dissolution/precipitation reactions in a manner consistent with the development of the solid microstructure. A previous publication describes the development of a stochastic, lattice-based reaction-transport model that is a promising candidate for modeling the the reactions and microstructural development leading to setting in cementitious materials [1, 2]. That model, called HydratiCA,‡ has been demonstrated to accurately simulate the diffusion of neutral or charged species in dilute and semi-dilute solutions [1]. It has also been shown to simulate the kinetics of simple unimolecular or bimolecular reactions, both homogeneously in solution and heterogeneously at solid-liquid interfaces [2]. Recently, HydratiCA has been used to clarify the mechanisms of the hydration of tricalcium silicate [3], a major component of portland cement. In contrast to earlier microstructure models developed specifically for cement paste hydration, such as CEMHYD3D [4] and μIC [5], the model formulation enables simulation of realistic chemical kinetics and thermodynamics and provides an intimate coupling to the development of microstructure.

Earlier studies using HydratiCA invoked several simplifying assumptions about the system for the sake of computational expediency. For example, to limit the number of coupled reactions that were simulated, those earlier studies intentionally neglected the formation of ion complexes in solution. In addition, past simulations necessarily have been confined to very small systems, no more than 1000 lattice sites with a lattice spacing of 1 μm, which is enough to model a single cement particle in solution. These small sizes are justifiable for investigating purely chemical kinetic effects. However, in cementitious materials and other complex porous media, the representative volume elements required to compute microstructure properties are much larger, typically by a factor of 100 or 1000. In such systems, the computational demands are so high for HydratiCA that it cannot be validated properly unless it is modified to run in parallel on multiple processors. Recently, this modification has been made, and we now use it to examine larger-scale systems than have been possible before.

‡ The name HydratiCA is a pseudo-acronym for Hydration by Cellular Automata.

In the next section, the model and its parallelization are described briefly. In the Results and Discussion section, we apply the model to several phenomena that are important in cement chemistry, including the influence of temperature and pH on the dissolution kinetics and equilibrium of portlandite, and the dissolution and equilibration of ettringite—a very sparingly soluble mineral in water. Finally, we report simulation results on the microstructural development of an idealized model of portland cement paste, and the development of spatial correlations between growing and dissolving condensed phases.

2. Modeling

The algorithms used in HydratiCA for modeling diffusion and chemical reactions are based on fundamental kinetic cellular automaton principles [6]. The details and basic verification of the algorithms are given elsewhere [1, 2]. The material microstructure is discretized on a regular cubic lattice having a lattice spacing of λ. The initial cement particle and water microstructure is mapped onto this lattice by assigning a phase (*e.g.*, $Ca(OH)_2$ or water) to each lattice site. These materials are themselves finely discretized into quanta of concentration called *cells*; the number of cells of a given material at a particular lattice point determines its local concentration.

Chemical changes and structural development are simulated by iterating over small time increments, each of which is decomposed into independent transport and reaction steps. Diffusion is modeled by allowing each cell at a lattice site to execute a random walk to a neighboring site. The probability p_t of the walk depends on the effective diffusivity D of the mobile species at the site and the length of the time increment τ being considered [1],

$$p_t = \frac{\tau D}{\lambda^2} \tag{1}$$

Similarly, probabilistic rules are formulated to simulate chemical reactions at a lattice site. The probability of the reaction occurring depends on the reaction rate constant and on the number of cells N_α of each reactant α that participates in the reaction. For example, the probability of occurrence of the i-th homogeneous reaction is given by [6]

$$p_{rx}^{(i)} = k\xi^{\left(\sum_\alpha \nu_\alpha^{(i)}\right)-1}\tau \prod_\alpha \max\left[0, \prod_{m=1}^{\nu_\alpha^{(i)}} N_\alpha - m + 1\right] \tag{2}$$

where ξ is a constant model parameter that relates N_α to the molar concentration of species α, and $\nu_\alpha^{(i)}$ is the molar stoichiometric coefficient of the reactant α participating in the reaction. Eq. (2) strictly applies only to homogeneous reactions. The same kind of equation applies for heterogeneous reactions and nucleation events, although the length scaling is somewhat different [2]. The reaction is allowed if $p_{rx}^{(i)}$ exceeds a random number $q \in [0, 1]$ drawn from a uniform distribution. If the reaction occurs at a lattice site, the number of cells of each reactant (product) is decremented (incremented) by the number

required by the molar stoichiometric coefficients of the reaction. Reactions that can proceed at appreciable rates in both forward and reverse directions are modeled as two separate one-way reactions. Both Eqs. (1) and (2) have been shown to converge, in the limit $\tau, \lambda \to 0$ to the standard rate equations for diffusion and homogeneous reactions, respectively [6].

Besides the molar stoichiometric coefficients for the reactants and products, each reaction is characterized by its absolute rate constant in either the forward or reverse direction, the solubility product or equilibrium constant at a reference temperature (taken to be 298 K unless stated otherwise), the activation enthalpy for either the forward or reverse reaction, the enthalpy of reaction, nucleation energy barriers (for heterogeneous reactions only), and stoichiometric coefficients of each reaction. These parameters are sufficient to capture the rate of reaction, the temperature dependence of the rate, and even the temperature dependence of the equilibrium state for reversible reactions [2]. In addition to these reaction parameters, several properties of each of the constituent substances are also required. For simple condensed phases like water and stoichiometric solids, the density, molar volume, and diffusion formation factor must be supplied. For mobile ionic solute species, one must provide the electrical charge, the diffusion coefficient at infinite dilution, and the Kielland ion-size parameters needed to calculate the activity coefficients using the extended Debye-Hückel equation. Values for many of these properties can be found in textbooks or other reference materials [7–10]. Unless stated otherwise, all equilibrium constants, Kielland ion-size parameters, and other thermodynamic data used in this paper are taken from the Nagra/PSI chemical thermodynamic database [11]. Finally, for non-stoichiometric solids, the model simulates compositional and structural variability by microscopic coprecipitation of two stoichiometric end member phases that span the desired range of compositions and physical properties, as described more fully in Ref. [3]. Each end member is assigned values for all the properties just listed, and then the relative rates of formation of each end member at a lattice site determines the local composition of the phase. An approach similar to this also is used in the thermodynamic modeling of non-stoichiometric solids [12].

2.1. Parallelization

Each lattice site in HydratiCA is occupied by numbers of cells of differing types, each of which represents a discrete concentration of a particular material component or phase. The algorithms used to compute changes in a site's cell occupation numbers require information only from the site and its nearest and next-nearest neighbor sites. This localization of the algorithms leads to a natural parallel decomposition of the simulation, by which the lattice is partitioned into sublattices, each of which is assigned to a separate computational *process*. Each process uses one CPU processor. A process *owns* each of the lattice sites of the sublattice it is assigned, and the owner of a lattice site is responsible for all of the computations needed to update that lattice site during each

time step of the simulation. Therefore, lattice sites that are on the surface of a sublattice must gather data from neighboring lattice sites that are owned by other processes. This updating is accomplished by surrounding each sublattice with a layer of "ghost" lattice sites that are images of the actual lattice sites owned by adjacent processes. In the simulations reported here, the lattice was decomposed into orthorhombic sublattices that were as close to the same size and as close to cubic as possible for the lattice shape and number of processes, in an effort to minimize the number of ghost lattice sites. Inter-process communication is handled using MPI (Message Passing Interface), the dominant communications protocol used in high-performance parallel computing [13].

If the communications needed to update the ghost lattice sites in each time step required no computational time (i.e. ideal communications), then simulations would scale perfectly up to the point at which each process owned a single lattice site. Because ideal communications are unattainable, parallel execution will be efficient only if each process owns enough lattice sites to make the overhead of communication time a small percentage of the overall simulation time.

HydratiCA's scaling behavior was examined using up to 448 processes on the Columbia supercomputer at the NASA Advanced Supercomputing Division (NASA/NAS). Fig. 1 (a) compares the multiplicative speed-up in identical simulations as a function of the number of processes. The simulations involved 17 types of cells with 12 coupled nonlinear reactions on a computational domain with $100 \times 100 \times 100$ lattice sites. Further details of the simulations are discussed in Section 3.3. In Fig. 1 (a), all timings are normalized by the timing for the simulation run on one processor. The figure indicates that HydratiCA can run effectively on this $100 \times 100 \times 100$ system using up to at least 448 processes. However, with increasing numbers of processes, the actual speed-up diverges from the ideal linear scaling, and that little or no performance is gained beyond 400 processes. This can be seen more clearly by plotting the same data in terms of the process efficiency, as shown in Fig. 1(b). Efficiency is defined here as the percentage of the simulation time that each process devotes to the actual simulation as opposed to inter-process communication.

It should be noted that the performance indicated in Fig. 1 is dependent on the number of lattice sites in the system and also on the chemical complexity, that is, the number of independent chemical components and chemical reactions that must be considered. If either the number of lattice points or the chemical complexity increases, the performance will scale better to higher numbers of processes than indicated in the figure, which was generated using a relatively simple chemical system.

3. Results and Discussion

3.1. Portlandite in Water: Effect of Temperature

To validate the model implementation on a relatively simple aqueous mineral system, we assume a one-step reaction for the reversible dissolution of portlandite, $Ca(OH)_2$, in

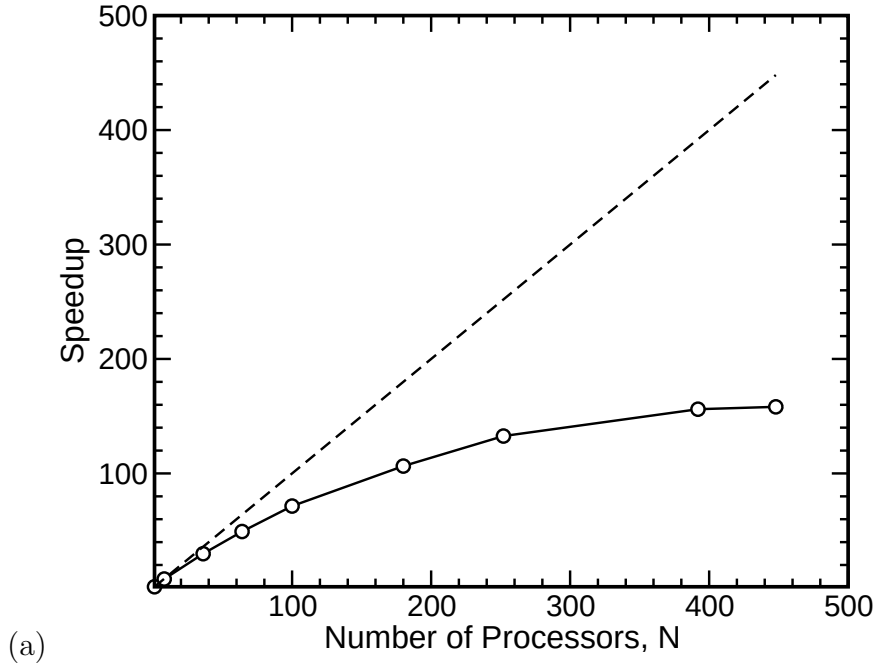

(a)

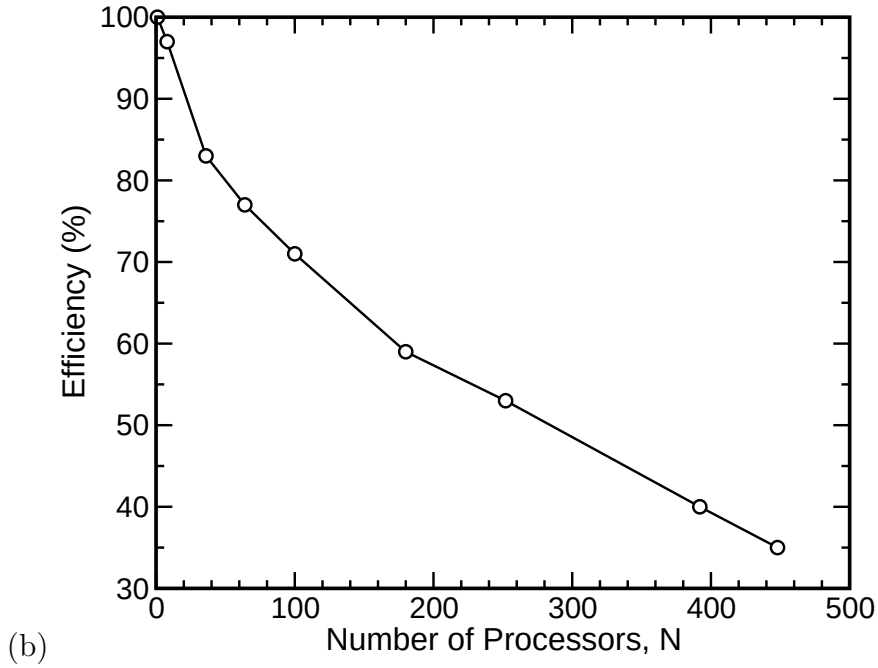

(b)

Figure 1. (a) Multiplicative speed-up factor for identical simulations as a function of number of processes. Simulations run on a $100 \times 100 \times 100$ lattice of ettringite particles in aqueous solution. The dashed line is the idealized linear scaling behavior. (b) Process efficiency for the same simulations as in (a), that is the percentage of process time devoted to computation as opposed to communication.

water, along with the speciation of calcium hydroxide in solution according to

$$\mathrm{Ca(OH)_2} \overset{k_1}{\rightleftharpoons} \mathrm{Ca^{2+}} + 2\,\mathrm{OH^-}\ , \log K_{\mathrm{sp}} = -5.20 \tag{3}$$

$$\mathrm{Ca^{2+}} + 2\,\mathrm{OH^-} \overset{k_2}{\rightleftharpoons} \mathrm{CaOH^+}\ , \log K_{\mathrm{eq}} = 1.22 \tag{4}$$

The values of the solubility product K_{sp} and complexation constant K_{eq} are those reported at 298 K in Ref [11]. We assume a dissociation rate constant of $k_1 = 7.2\ \mu\mathrm{mol}/(\mathrm{m}^2 \cdot \mathrm{s})$, inferred from published studies of the kinetics of portlandite crystal growth [14]. Also based on that data, we assume an activation enthalpy for portlandite dissolution of $\Delta H_1^* = 57.5$ kJ/mol. The enthalpy of dissociation is $\Delta H_1 = -17.06$ kJ/mol. A value for the enthalpy of the complexation reaction could not be found in any of the thermodynamic databases we searched, perhaps because the heat capacity and its temperature dependence for $\mathrm{CaOH^+}$ have not been measured. Here we assume a value of $\Delta H_2 = -2.16$ kJ/mol, which is comparable to the enthalpies of similar speciation reactions [12]. Similarly, we have not found a published value of the rate constant k_2 for formation of the $\mathrm{CaOH^+}$ complex; however, complexation reactions in solution generally equilibrate rapidly compared with mineral dissociation and growth [15]. In the absence of any data, we chose to set the rate constant considerably greater than k_1 to promote near-equilibrium conditions in solution. However, if the rate constant is set too high, smaller time steps are required to maintain stability of the algorithm embodied in Eq. (2). Through a series of test simulations, we found that a rate constant $k_2 = 16.6\ \mathrm{mol}/(\mathrm{m}^3 \cdot \mathrm{s})$, was great enough to maintain near-equilibrium conditions in solution without requiring significantly smaller time steps.

The system, shown in Fig. 2, is a cubic volume 100 μm on each side, with a lattice spacing of 1 μm, containing a suspension of portlandite particles suspended in pure water. The initial solid volume fraction is 0.237, and the initial specific surface area of the solid is 1.43 $\mu\mathrm{m}^2/\mu\mathrm{m}^3$, which corresponds to a mean equivalent spherical diameter of 4.2 μm.

Figure 3 shows the predicted total calcium concentration as a function of time at 293 K, 298 K, and 303 K. The data follow the expected qualitative trends. That is, the initial rate of dissolution increases with temperature, as expected for any thermally activated process. In addition, the total calcium concentration near equilibrium decreases with increasing temperature, also as expected for any net exothermic dissolution process. Quantitatively, the initial rate of dissolution, calculated from the limiting value of the slopes at zero time in Fig. 3, are shown in Table 1 and compared with the "target" value that is inferred from the assumed values of k_1 and ΔH_1^*. The calculated rate at 293 K exceeds the true rate by only 3.5 %, and the discrepancy decreases with increasing temperature, although at the two higher temperatures the calculated initial rates are slightly lower than the expected values.

To more clearly depict the accuracy with which the model predicts the equilibrium state of the system, the inset of Fig. 3 compares the near-equilibrium total calcium

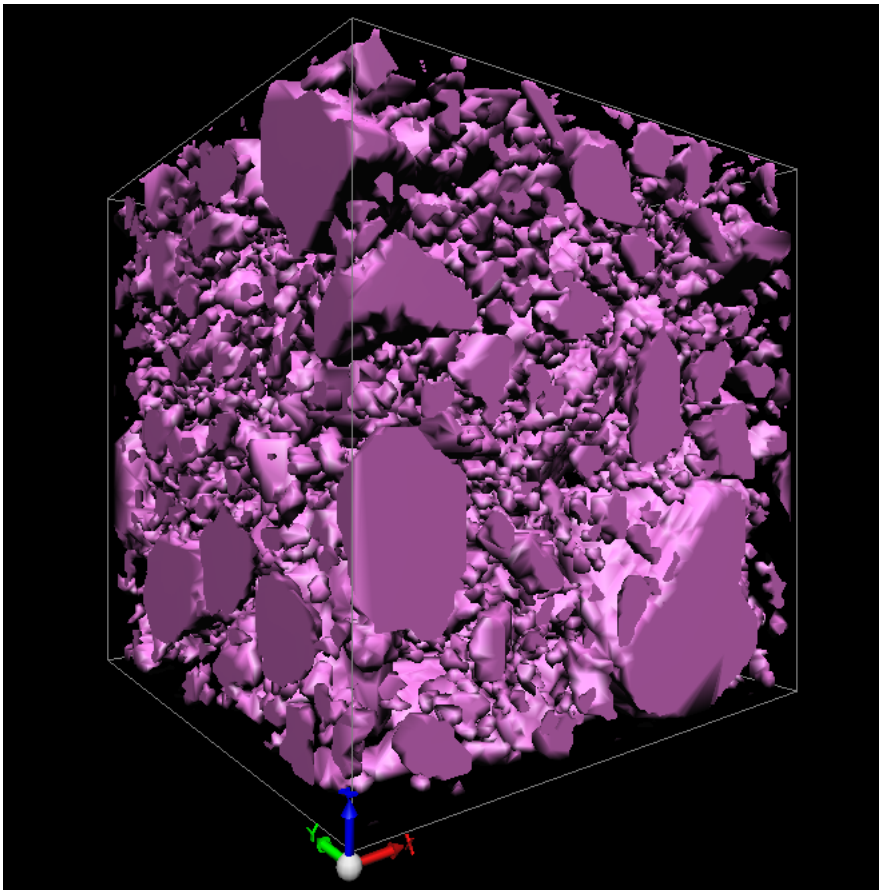

Figure 2. Suspension of portlandite particles suspended in water. The cubic lattice is 100 μm on each side, with a lattice spacing of 1 μm.

Table 1. Comparison of calculated and target initial dissolution rates of portlandite in water at 293 K, 298 K, and 303 K.

T (K)	**Calculated Rate** ($\mu\text{mol} \cdot \text{m}^{-2} \cdot \text{s}^{-1}$)	**Target Rate** ($\mu\text{mol} \cdot \text{m}^{-2} \cdot \text{s}^{-1}$)	**Difference** (%)
293	5.00	4.83	3.5 %
298	7.00	7.19	-2.6 %
303	10.50	10.51	-0.1 %

concentration, $[Ca^{2+}] + [CaOH^{+}]$, (solid) with the recommended values (dashed) published by the International Union of Pure and Applied Chemistry [16]. The greatest discrepancy, occurring at 293 K, is 0.9 mmol/L or 4 %. We also have compared the total calcium concentration, as well as $[Ca^{2+}]$ and $[CaOH^{+}]$ individually, to the values predicted by the GEMS-PSI thermodynamic modeling software package [17], which uses the Nagra/PSI thermodynamic database [11]. Again, the maximum discrepancy is less than 1 mmol/L (about 4 %) and occurs at 293 K.

It is important to note that different thermodynamic modeling software packages

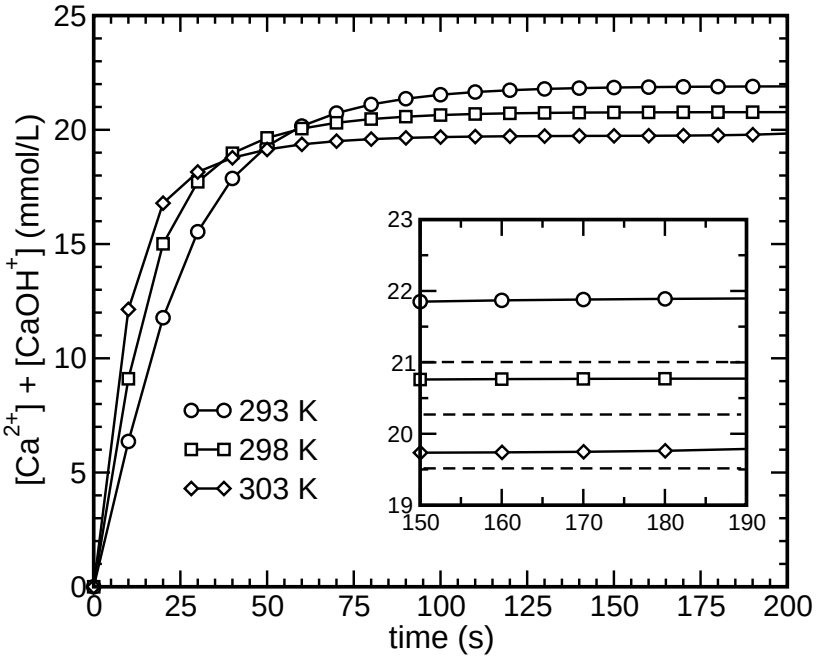

Figure 3. Prediction of the time dependence of the total calcium concentration in solution for dissolution of portlandite in pure water at 298 K. Dashed lines in the inset represent experimentally measured values of equilibrium total calcium concentration reported in [16].

and databases may not agree on the equilibrium state of a system, even for one as simple as portlandite in water. For example, the thermodynamic calculations just described were repeated with the PHREEQC thermodynamic modeling software package using the LLNL and WATEQ4 databases, hereafter referred to collectively as P/LW. At 298 K , P/LW agrees to within 1 mmol/L with the cited experimental data, with the GEMS software package calculation, and with the HydratiCA calculation of total calcium concentration. However, at 293 K, P/LW calculates a total calcium concentration of 29 mmol/L, which is about 7 mmol/L, or about 33 %, higher than either the experimental value, the value calculated by GEMS, or the value predicted by HydratiCA. Similarly, at 303 K, P/LW calculates a total calcium concentration of 14 mmol/L, which is about 6 mmol/L, or about 30 %, lower than any of the other values. Clearly, the temperature dependence predicted by P/LW near 298 K for this system, although in the correct direction, is much too severe, and is most likely due to its approximation of activity coefficients using the Davies equation instead of the extended Debye-Hückel equation as implemented by GEMS and by HydratiCA.

3.2. Portlandite in Water: Effect of pH

In portland cement pastes, the solution in the capillary pore space typically has a high pH (12 to 13), the value depending in part on the concentration of readily soluble alkali salts in the cement. Therefore, it is important for a model of cement hydration to

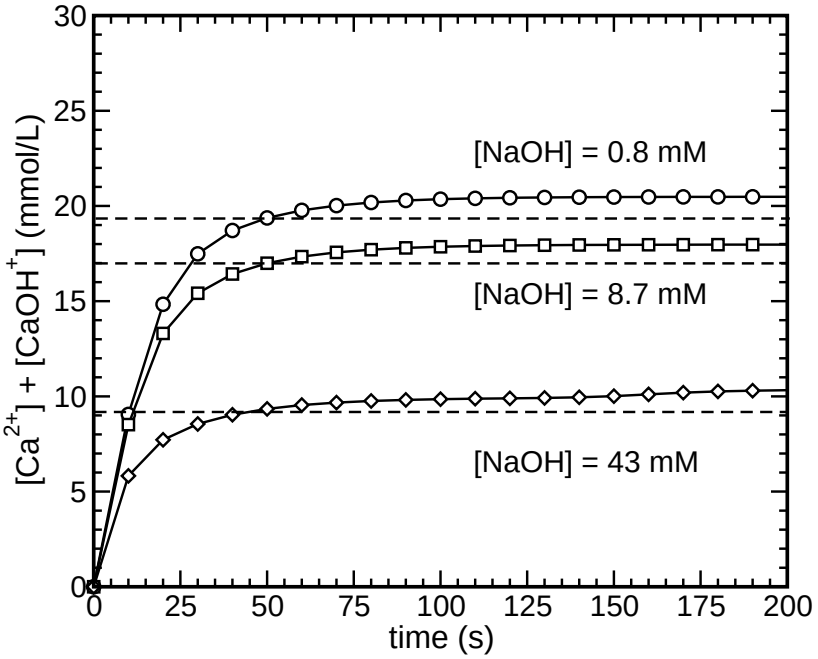

Figure 4. Prediction of the time dependence of the total calcium concentration in solution for dissolution of portlandite in pure water. Dashed lines indicate expected equilibrium total calcium concentrations calculated by GEMS-PSI thermodynamic modeling software [17].

adequately capture the effect of solution pH on the dissolution kinetics and equilibrium solubility of minerals. As a prototype example, we consider the behavior of portlandite in aqueous solutions of NaOH. The same system is used as in the last section, except that the particles are now suspended in an aqueous solution of NaOH at concentrations of either 0.87 mmol/L, 8.7 mmol/L, or 43 mmol/L at a constant temperature of 298 K. In addition to reactions (3) and (4), we also need to consider the formation of the $NaOH^0$ complex in solution according to

$$Na^+ + OH^- \overset{k_3}{\underset{}{\rightleftharpoons}} NaOH^0 \ , \log K_{eq} = -0.18 \tag{5}$$

Again, to ensure that this complexation reaction is sufficiently rapid to keep it from being rate-controlling, we assume $k_3 = 16.6$ mol/(m$^3 \cdot$ s), the same value used for the $CaOH^+$ complexation reaction.

Figure 4 shows the time dependence of the total calcium concentration at three different NaOH concentrations. The first noteworthy feature of the plot is the near-equilibrium predictions of total calcium concentration, compared to expected values calculated by GEMS-PSI (dashed lines). The simulation values exceed the expected values by about 0.001 mmol/L at all three concentrations. The reason for this small but systematic discrepancy is not known, although it appears to be about the same magnitude and sign as for portlandite in pure water from the last section.

As a check on the kinetic behavior, the instantaneous rate of dissolution at zero time is expected to be exactly the same as in the absence of NaOH because $[Ca^{2+}]$, and

therefore the ionic activity product (IAP) for portlandite, is still zero initially. Indeed, the mean dissolution rate over the first 0.5 s of dissolution is equal to the predicted value in the second column of Table 1 at 298 K. It is clear from Fig. 4, however, that the rates become unequal within seconds, which also is expected because increased concentrations of OH^- with increasing concentrations of NaOH result in a higher IAP as soon as the concentrations of the other species are nonzero.

3.3. Solubility of Ettringite in Water

Having validated the model implementation in terms of the influence of temperature and pH variations on a simple mineral, we now test the model on a more chemically complex mineral. For this purpose, we choose the mineral ettringite, for which the dissociation reaction may be modeled as [12]

$$\begin{aligned} &Ca_6Al_2(SO_4)_3(OH)_{12}{\cdot}26\,H_2O \\ &\quad \overset{k_4}{\rightleftharpoons} 6\,Ca^{2+} + 2\,Al(OH)_4^- + 3\,SO_4^{2-} + 4\,OH^- + 26\,H_2O\ , \log K_{sp} = -45.09 \end{aligned} \quad (6)$$

which has a reaction enthalpy of $\Delta H_4 \approx 204.5$ kJ/mol at 298 K [12, 18]. Ettringite is an important mineral in portland cement both as a product of the reaction between tricalcium aluminate and calcium sulfate, and also at later times where it participates in chemical degradation processes [8]. It provides a good test of the model because its solubility product is nearly 40 orders of magnitude lower than that of portlandite. The concentrations of calcium and hydroxyl ions in solution are both an order of magnitude less than the equilibrium concentrations for portlandite and, in addition, aluminate and sulfate ions are also present in even lower concentrations. Thermodynamic modeling calculations indicate that more than a dozen solute species should be present in solution at equilibrium with ettringite, six of which—Ca^{2+}, $CaOH^+$,SO_4^{2-}, $CaSO_4^0$, $Al(OH)_4^-$, and OH^-—should be present in greater than trace concentrations. Therefore, we must account for a second speciation reaction, in addition to reaction (4),

$$Ca^{2+} + SO_4^{2-} \overset{k_5}{\rightleftharpoons} CaSO_4^0\ , \log K_{eq} = 2.44 \quad (7)$$

In the absence of reported rate data, we once again assume $k_5 = 16.6$ mol/(m$^3 \cdot$ s)to prevent this speciation reaction from being rate-controlling.

The system used is the same as shown in Fig. 2, except that the solid phase is now identified as ettringite instead of portlandite. Table 2 shows the near-equilibrium concentrations of solute components at 298 K and compares them to the concentrations predicted by the GEMS-PSI thermodynamic modeling application [17] assuming the same solubility product. It should be noted that solid $Al(OH)_3$, gibbsite, is thermodynamically expected to precipitate in small quantities. However, for the purposes of this calculation we have neglected the formation of gibbsite both in HydratiCA and in the thermodynamic calculations. As the table indicates, the predicted concentrations are well-matched to the thermodynamic calculations, with no more than

Table 2. Comparison of calculated and expected values of the solute concentrations in equilibrium with ettringite at 298 K, neglecting the possibility of gibbsite formation.

Component	**Calculated** (mmol/L)	**Expected** (mmol/L)	**Difference** (mmol/L)
Ca^{2+}	1.83	1.80	0.03
OH^-	1.31	1.29	0.02
SO_4^{2-}	0.85	0.84	0.01
$Al(OH)_4^-$	0.67	0.66	0.01
$CaSO_4^0$	0.16	0.16	0.00
$CaOH^+$	0.04	0.03	0.01

a 0.03 mmol/L absolute difference. The values given in Table 2 also are consistent with the range of solution compositions found in available experimental studies [19–22]. Therefore, even for sparingly soluble minerals that may be in equilibrium with solute components at concentrations as low as several μmol/L, the model implementation provides good calculations of equilibrium and kinetics.

3.4. Phase Correlations in Hydrating Cement Paste

By tracking the development of the microstructure of a 3-D system, one could begin to investigate spatial correlations between growing and dissolving phases. Some solute species in cement, like aluminate ions, are added to solution by dissolution of tricalcium aluminate (C_3A)§ and tetracalcium aluminoferrite (C_4AF), but not by tricalcium silicate (C_3S). These aluminate ions are needed for the growth of minerals like ettringite or calcium monosulfoaluminate, but not for portlandite. Silicate ions are added to solution by dissolution of C_3S and C_2S, but not from C_3A or C_4AF, and are needed for the growth of calcium silicate hydrate gel (C–S–H) but not portlandite or ettringite. Therefore, a hydrating cement paste is composed of a set of coupled reaction networks, similar to those being studied in biological systems [23, 24], and the topology of these networks, along with the transport rates of the solute species, may give rise to spatial correlations between different dissolving and growing phases in cement paste.

As an example, we conclude with a preliminary result for a system composed of C_3S, C_3A, and gypsum ($CaSO_4{\cdot}2\ H_2O$) suspended in water, as shown in Fig. 5(a). This represents a highly idealized portland cement paste. The microstructure at time $t = 0$ is shown in Fig. 5(a), and the assumed reactions are given in Table 3. The total solid volume fraction of the system is 0.32, which is somewhat more dilute than typical portland cement binders in concrete.

As the initial particles dissolve, solid hydration products are formed. In particular,

§ In this section, we adopt conventional cement chemistry notation by which single letters are used to denote simple oxide components of cement minerals, e.g. C = CaO, A = Al_2O_3, F = Fe_2O_3, S = SiO_2, H = H_2O.

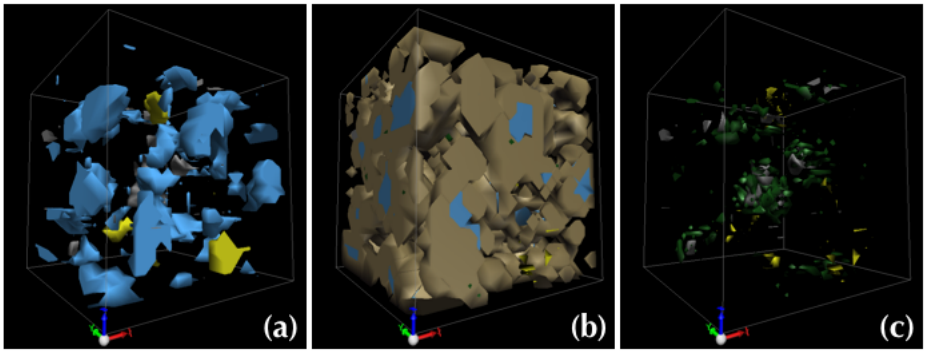

Figure 5. Simulated suspension of tricalcium silicate, tricalcium aluminate, and calcium sulfate dihydrate in water: (a) initial suspension microstructure, (b) microstructure after three hours of hydration, and (c) same microstructure with silicate phases subtracted to reveal the calcium sulfate and calcium aluminate phases more clearly. The color scheme is: light blue = C_3S, light brown = C–S–H, dark blue = portlandite, gray = C_3A, yellow = gypsum, green = ettringite.

calcium silicate hydrate and portlandite are possible hydration products of the dissolution of C_3S (see reactions 1,4–6 in Table 3). Ettringite and portlandite are possible hydration products formed by the dissolution of C_3A and gypsum (see reactions 2,3,6, and 7 in Table 3). These two reaction networks are coupled through Ca^{2+} and OH^- ions in solution, which are common to both networks.

Because $Al(OH)_4^-$ and $H_2SiO_4^{2-}$ have lower intrinsic diffusion coefficients in water than Ca^{2+}, OH^-, or SO_4^{2-}, one might expect to observe ettringite to form in the vicinity of C_3A, and C–S–H to form in the neighborhood of C_3S, the sources of $Al(OH)_4^-$ and $H_2SiO_4^{2-}$, respectively.

A growing body of experimental [25–27] and modeling [3, 28] evidence strongly suggests that C–S–H nucleates heterogeneously on the surfaces of C_3S, so in this simulation the nucleation barrier for C–S–H on C_3S was set low enough to encourage C–S–H nucleation exclusively on C_3S surfaces. Therefore, a strong spatial correlation between C–S–H and C_3S is expected to arise due to nucleation effects. However, neither portlandite nor ettringite are assumed to nucleate preferentially on any solid surfaces, so the locations of their precipitation should be dictated only by the relative abundance of solute species from which they form. In fact, the preliminary results of this simulation indicate that the locations of ettringite and portlandite are strongly correlated with C_3A, but are not correlated significantly with either C_3S or gypsum. This can be seen visually in Fig. 5(c), where the proximity of ettringite crystals to tricalcium aluminate is readily observed. To probe the effect quantitatively, radial distribution functions (RDF) for both ettringite and portlandite were calculated from the simulated microstructure at 3 h of hydration. The RDF of a phase i gives the ratio of the concentration of that phase to its average concentration, $\phi_i(r)/\langle\phi_i\rangle$ as a function of distance r from a reference point. Fig. 6 plots the RDF for portlandite using surfaces of C_3A, C_3S, or gypsum as the reference point. For example, the curve with the circular points is the radial distribution

Table 3. Summary of assumed reactions and reaction parameters for hydration of idealized portland cement. k_+ is the reaction rate constant in the forward direction (left to right) for each reaction.

	Reaction	k_+ (298 K) $(\mathrm{mol}/(\mathrm{m}^2 \cdot \mathrm{s}))$	$\log K_{eq}$
1	$Ca_3SiO_5 + 3\,H_2O \rightleftharpoons 3\,Ca^{2+} + H_2SiO_4^{2-} + 4\,OH^-$	5.2×10^{-7}	-17.0
2	$Ca_3Al_2O_6 + 6\,H_2O \rightleftharpoons 3\,Ca^{2+} + 2\,Al_2O_4^- + 4\,OH^-$	2.0×10^{-6}	-10.3
3	$CaSO_4{\cdot}2\,H_2O \rightleftharpoons Ca^{2+} + SO_4^{2-} + 2\,H_2O$	2.0×10^{-5}	-4.48
4	$C{-}S{-}H(I) \rightleftharpoons Ca^{2+} + H_2SiO_4^{2-} + 3\,H_2O$	4.2×10^{-7}	-7.52
5	$C{-}S{-}H(II) \rightleftharpoons 2\,Ca^{2+} + H_2SiO_4^{2-} + 2\,OH^- + 3\,H_2O$	5.0×10^{-7}	-12.96
6	$Ca(OH)_2 \rightleftharpoons Ca^{2+} + 2\,OH^-$	7.2×10^{-6}	-5.2
7	$C_3A{\cdot}3\,CaSO_4{\cdot}32\,H_2O \rightleftharpoons 6\,Ca^{2+} + 3\,SO_4^{2-} + 2\,Al(OH)_4^-$ $+4\,OH^- + 26\,H_2O$	1.0×10^{-19}	-45.1
8	$C_3A{\cdot}CaSO_4{\cdot}12\,H_2O \rightleftharpoons 4\,Ca^{2+} + SO_4^{2-} + 2\,Al(OH)_4^-$ $+4\,OH^- + 6\,H_2O$	1.0×10^{-14}	-29.3
9	$C_4AH_{19} \rightleftharpoons 4\,Ca^{2+} + 2\,Al(OH)_4^- + 6\,OH^- + 12\,H_2O$	1.0×10^{-9}	-25.6
10	$Al(OH)_3 + OH^- \rightleftharpoons Al(OH)_4^-$	2.22	-0.24
11	$CaOH^+ \rightleftharpoons Ca^{2+} + OH^-$	0.063	-1.2
12	$CaSO_4^0 \rightleftharpoons Ca^{2+} + SO_4^{2-}$	0.063	-2.1
13	$C_3A + CaSO_4^0 \rightleftharpoons C_3A + CaSO_4(ads)$	0.063	-2.1

function using C_3A surfaces as the reference point, averaged over all of the C_3A surface sites in the microstructure. Fig. 7 gives the RDFs calculated for ettringite using the same three surfaces as reference points.

Figs. 6 and 7 show that both portlandite and ettringite are strongly correlated with C_3A surfaces. The concentrations of these phases near C_3A are about 2.5 times their average concentrations throughout the microstructure. Furthermore, the RDF of both phases decays rapidly with distance, reaching a minimum value at about 8 μm, where both phases are relatively depleted compared to their average concentrations. The location of the minimum at 8μm corresponds closely to the average spacing of C_3A domains in the microstructure, as shown by plotting the autocorrelation function for C_3A (Fig. 8). The first minimum of the autocorrelation function is the average spacing of C_3A domains [29]. Therefore, the increase in the RDF at distances greater than 8 μm is likely due to the approach of another C_3A surface.

In contrast to their strong correlation with C_3A surfaces, neither portlandite nor ettringite are strongly correlated with C_3S or gypsum surfaces; the RDF departs only slightly from unity at any distance from these surfaces. The fact that ettringite is not strongly correlated to gypsum indicates that SO_4^{2-} ions are sufficiently mobile that they do not limit the formation of ettringite. Portlandite, which is a product of the hydration

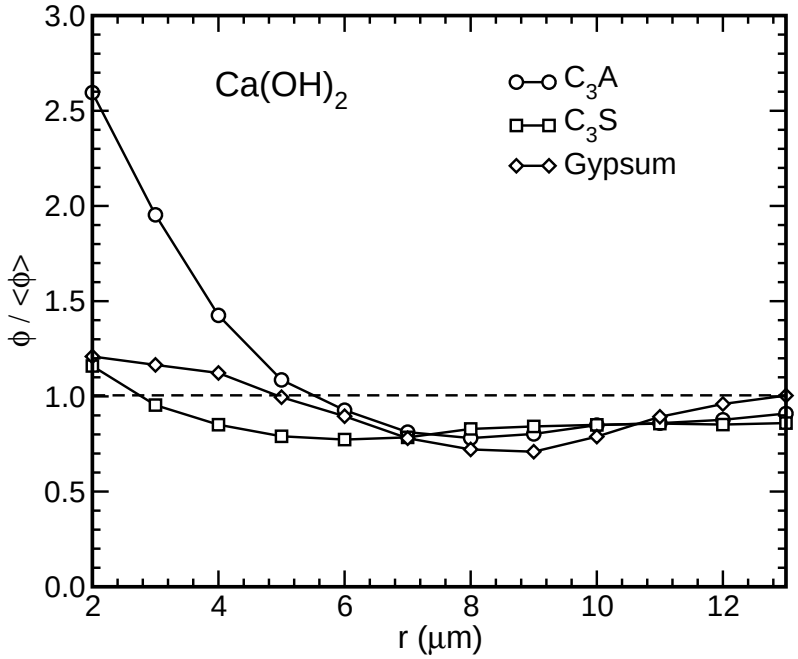

Figure 6. Calculated radial distribution functions for portlandite using C_3A, C_3S, or gyspum surfaces as the reference point, for the microstructure shown in Fig. 5(b). The standard deviation of the sample mean at each distance is less than 0.07, about the size of each point.

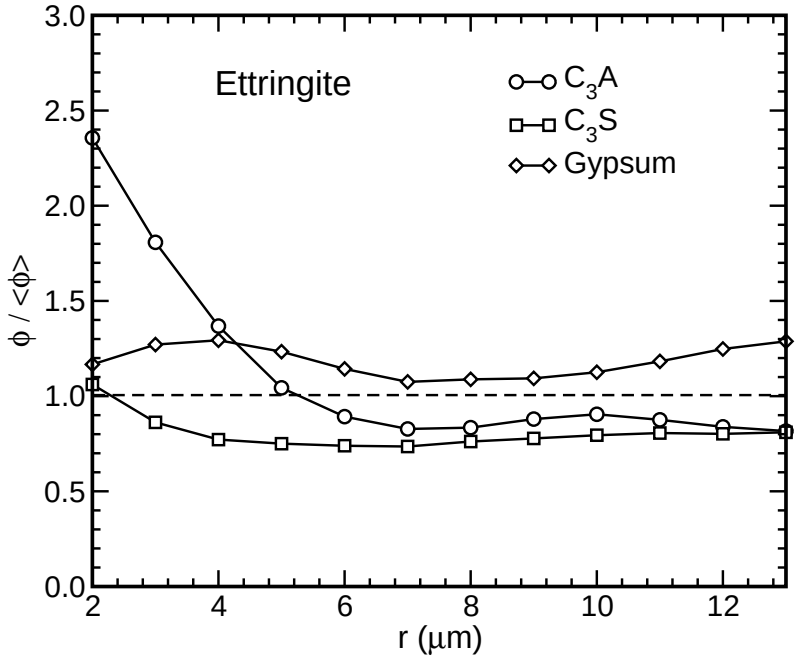

Figure 7. Calculated radial distribution functions for ettringite using C_3A, C_3S, or gyspum surfaces as the reference point, for the microstructure shown in Fig. 5(b). The standard deviation of the sample mean at each distance is less than 0.07, about the size of each point.

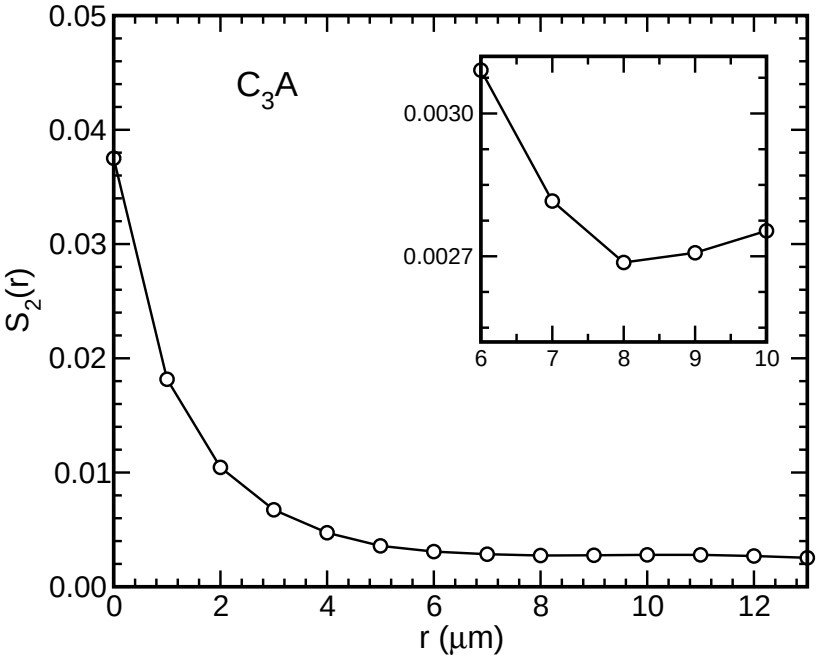

Figure 8. Calculated autocorrelation function for C_3A for the microstructure in Fig. 5(b). The inset shows a magnified view of the first minimum in the autocorrelation curve, which is interpreted as the average spacing of C_3A domains.

both of C_3S and of C_3A, is not strongly correlated to C_3S because silicate ions are not required to form it. In addition, volume exclusion due to the presence of C–S–H near the C_3S surfaces seems to prevent portlandite from forming as abundantly near C_3S as it does near C_3A.

These kinds of spatial correlations among phases are now being investigated experimentally using scanning electron microscopy coupled with energy dispersive spectroscopy (EDS) to test the predictions made by HydratiCA [30]. A strong coupling of experiment and simulation will help determine what, if any, general statements can be made about the reaction network topology and spatial correlations in microstructures as complex as those found in hydrating cement pastes.

4. Summary

A lattice-based cellular automaton model has been described for simulating 3-D microstructure development under multiple coupled nonlinear reactions and diffusive mass transport. The algorithms applied at each lattice site require information only from the site itself and its neighboring lattice sites. The localized nature of the calculations enable the model to be parallelized to run on multiple processors. For the model system size investigated here, the simulation speed scales well up to 100 processes, but the scaling behavior diverges significantly from linear for higher process numbers. Likewise, the computational efficiency decreases nearly linearly up to 448 processes, where inter-process communications reach 65 % of the total process time.

HydratiCA is a general model that should be applicable to a diverse range of reactive systems, including porous geochemical environments and biochemical phenomena inside living cells. Here we have focused on systems relevant to hydrating cementitious materials, providing several points of verification and validation of the implementation on aqueous suspensions of portlandite and ettringite. The model accurately captures the effects of temperature and pH on the kinetics and equilibria of the dissociation of minerals like portlandite in water. In at least one instance, the simulations give significantly better agreement to experimental measurements than the PHREEQC software package using the LLNL and WATEQ4 databases. More chemically complex minerals like ettringite, with exceedingly small solubility products, are simulated with an accuracy that is comparable to the range of measured or calculated solubilities that have been reported previously.

The coupling of realistic chemical kinetics and thermodynamics to 3-D microstructure enables HydratiCA to directly incorporate the effects of particle size distribution, particle shape, and surface area into its calculations. In addition, the model can be used to investigate the emergence of spatial correlations between growing and dissolving phases in complex 3-D microstructures like those found in hydrating cement pastes. Preliminary results for an idealized portland cement paste were shown in this paper, but more systematic experimental and computational investigations are currently underway.

Minerals like portlandite, gypsum, and ettringite tend to have extremely anisotropic growth rates in cement paste, leading to crystal morphologies that are tabular or acicular with aspect ratios approaching 100. The current implementatin of HydratiCA does not account for growth anisotropy in any way, but it could do so by making the growth probability a function of the unit normal vector to the interface at each lattice site where growth occurs. The form of this function could be taken from polar plots of the so-called growth mobility function which is used in the geometric theory of crystal growth [31].

Acknowledgments

This work was supported by the Virtual Cement and Concrete Testing Laboratory Consortium and by the Partnership for High-Performance Concrete Technology program (HYPERCON) at the National Institute of Standards and Technology. Large-scale parallel computations were performed under Award SMD-05-A-0129, for NASA's National Leadership Computing System initiative on the "Columbia" supercomputer at the NASA Ames Research Center. The authors are indebted to Barbara Lothenbach for insightful comments about thermodynamic calculations of solubility, and to Ken Snyder, Ed Garboczi, and Jeff Thomas for thoughtful critiques of the manuscript.

References

[1] Bullard J W 2007 Approximate rate constants for nonideal diffusion and their application in a stochastic model *J. Phys. Chem. A* **111** (11) 2084–2092

[2] Bullard J W 2007 A three-dimensional microstructural model of reactions and transport in aqueous mineral systems *Modelling Simulation in Mater. Sci. Eng.* **15** 711–738

[3] Bullard J W 2008 A determination of hydration mechanisms for tricalcium silicate using a kinetic cellular automaton model *J. Am. Ceram. Soc.* **91** (7) 2088–2097

[4] Bentz D P 1997 Three-dimensional computer simulation of cement hydration and microstructure development *J. Am. Ceram. Soc.* **80** (1) 3–21

[5] Bishnoi S and Scrivener K L 2009 μic: A new platform for modelling the hydration of cements *Cem. Concr. Res.* **39** (4) 266–274

[6] Karapiperis T and Blankleider B 1994 Cellular automaton model of reaction-transport processes *Physica D* **78** 30–64

[7] Langmuir D 1997 *Aqueous Environmental Geochemistry* (London, England: Prentice-Hall)

[8] Taylor H F W 1997 *Cement Chemistry* (London: Thomas Telford) 2nd edition

[9] Parkhurst D L 1995 User's guide to PHREEQC—a computer program for speciation reaction-path, advective-transport, and geochemical calculations Water-Resources Investigations Report 95-4227 U.S. Geological Survey

[10] Mills R and Lobo V M M 1989 *Self-Diffusion in Electrolyte Solutions* (Amsterdam: Elsevier)

[11] Hummel W, Berner U, Curti E, Pearson F J and Thoenen T 2002 *Nagra / PSI Chemical Thermodynamic Data Base 01/01* (Parkland, Florida: Universal Publishers)

[12] Lothenbach B and Winnefeld F 2006 Thermodynamic modelling of the hydration of Portland cement *Cem. Concr. Res.* **36** 209–226

[13] Pacheco P 1996 *Parallel Programming with MPI* (San Francisco, CA: Morgan Kaufmann)

[14] Tadros M E, Skalny J and Kalyoncu R S 1976 Kinetics of calcium hydroxide crystal growth from solution *J. Colloid Interface Sci.* **55** (1) 20–24

[15] Lasaga A C 1981 Rate laws of chemical reactions in A C Lasaga and R J Kirkpatrick (eds.) *Kinetics of Geochemical Processes* (Mineralogical Society of America) number 8 in Reviews in Mineralogy pp. 1–68

[16] Lambert I and Clever H L (eds.) 1992 *Alkaline Earth Hydroxides in Water and Aqueous Solutions (Solubility Data Series)* volume 52 (Oxford, England: International Union of Pure and Applied Chemistry, Pergamon Press)

[17] Kulik D A 2002 GEMS-PSI 2.0 http://les.web.psi.ch/Software/GEMS-PSI/

[18] Thomas J J, Rothstein D, Jennings H M and Christensen B J 2003 Effect of hydration temperature on the solubility behavior of Ca-, S-, Al-,and Si-bearing solid phases in Portland cement pastes *Cem. Concr. Res.* **33** 2037–2047

[19] Lea F M 1970 *The Chemistry of Cement and Concrete* (Edward Arnold) 3rd edition

[20] Ghorab H Y and Kishar E A 1985 Studies on the stability of calcium sulfoaluminate hydrates. part 1: Effect of temperature on the stability of ettringite in pure water *Cem. Concr. Res.* **15** 93–99

[21] Atkins M, Glasser F, Kindness A, Bennett D, Dawes A and Read D 1991 A thermodynamic model for blended cements DoE Report DoE/HMIP/RR/92/005 U.S. Department of Energy

[22] Zhang F, Zhou Z and Lou Z 1997 Solubility product and stability of ettringite in *Proceedings of the Tenth International Congress on the Chemistry of Cement* (Göteborg, Sweden) pp. II–88–I–93

[23] Alon U 2003 Biological networks: The tinkerer as an engineer *Science* **301** 1866–1867

[24] Alon U 2007 Simplicity in biology *Nature* **446** 497

[25] Garrault-Gauffinet S and Nonat A 1999 Experimental investigation of calcium silicate hydrate (C-S-H) nucleation *J. Cryst. Growth* **200** 565–574

[26] Garrault S and Nonat A 2001 Hydrated layer formation on tricalcium and dicalcium silicate surfaces: Experimental study and numerical simulations *Langmuir* **17** 8131–8138

[27] Garrault S, Finot E, Lesniewska E and Nonat A 2005 Study of C–S–H growth on C_3S surface during its early hydration *Mater. Structures* **38** 435–442
[28] Thomas J J 2008 A new approach to modeling the nucleation and growth kinetics of tricalcium silicate hydration *J. Am. Ceram. Soc.* **90** (10) 3282–3288
[29] Berryman J G and Blair S C 1986 Use of digital image analysis to estimate fluid permeability of porous materials: Application of two-point correlation functions *J. Appl. Phys.* **60** (6) 1930–1938
[30] Snyder K A 2009 Personal communication
[31] Taylor J E, Cahn J W and Handwerker C A 1992 Overview 1. Geometric models of crystal growth *Acta Metall. Mater.* **40** (7) 1443–1474